



# One-step in situ solvothermal synthesis of SnS<sub>2</sub>/TiO<sub>2</sub> nanocomposites with high performance in visible light-driven photocatalytic reduction of aqueous Cr(VI)

Yong Cai Zhang<sup>a,\*</sup>, Jing Li<sup>a</sup>, Hai Yan Xu<sup>b</sup>

<sup>a</sup> Key Laboratory of Environmental Material and Environmental Engineering of Jiangsu Province, College of Chemistry and Chemical Engineering, Yangzhou University, Yangzhou 225002, China

<sup>b</sup> School of Materials & Chemical Engineering, Anhui University of Architecture, Hefei 230022, China

## ARTICLE INFO

### Article history:

Received 26 January 2012

Received in revised form 11 April 2012

Accepted 15 April 2012

Available online 21 April 2012

### Keywords:

SnS<sub>2</sub> and TiO<sub>2</sub>  
Nanocomposites  
Cr(VI) reduction  
Photocatalysis  
Stability

## ABSTRACT

SnS<sub>2</sub>/TiO<sub>2</sub> nanocomposites with adjustable TiO<sub>2</sub> contents were synthesized directly via the solvothermal reactions of SnCl<sub>4</sub>·5H<sub>2</sub>O, thioacetamide and different amounts of tetrabutyl titanate in the mixed solvents of ethanol and acetic acid at 180 °C for 12 h. The structures, compositions, Brunauer–Emmett–Teller (BET) specific surface areas and optical properties of the as-synthesized products were characterized by X-ray diffraction, energy dispersive X-ray spectroscopy, X-ray photoelectron spectroscopy, field emission scanning electron microscopy, high resolution transmission electron microscopy, N<sub>2</sub> adsorption and UV–vis diffuse reflectance spectra, and their photocatalytic properties were tested for the reduction of aqueous Cr(VI) under visible light ( $\lambda > 420$  nm) irradiation. Furthermore, contrast photocatalytic experiments were also conducted for different doses of the as-synthesized SnS<sub>2</sub>/TiO<sub>2</sub> nanocomposite, SnS<sub>2</sub> and physical mixture of SnS<sub>2</sub> and TiO<sub>2</sub>. It was found that the as-synthesized SnS<sub>2</sub>/TiO<sub>2</sub> nanocomposite with a suitable TiO<sub>2</sub> content (e.g., 44.5 mass% TiO<sub>2</sub>) not only exhibited extraordinary superior photocatalytic activity to SnS<sub>2</sub>, TiO<sub>2</sub> and physical mixture of SnS<sub>2</sub> and TiO<sub>2</sub> (44.5 mass%) at different catalyst doses, but also had good photocatalytic stability. Moreover, Cr(VI) can be reduced to Cr(III) by SnS<sub>2</sub>/TiO<sub>2</sub>-mediated photocatalysis. The tight heterojunction structure of the as-synthesized SnS<sub>2</sub>/TiO<sub>2</sub> nanocomposite, which can facilitate interfacial electron transfer and reduce the separation and self-agglomeration of two components, was considered to play an important role in achieving its greatly improved photocatalytic performance.

© 2012 Elsevier B.V. All rights reserved.

## 1. Introduction

Cr(VI) is a frequent contaminant in wastewaters arising from industrial processes such as leather tanning, electroplating, mining and chromate manufacturing, etc. It is toxic to most organisms and has been classified as carcinogenic and mutagenic. Due to its high toxicity and high mobility in water, Cr(VI) has been included in the list of priority pollutants and its maximum concentrations in drinking water and discharged industrial wastewaters have been regulated by many countries of the world, for example, the allowable limits of Cr(VI) in drinking water and discharged industrial wastewaters in China are 0.05 and 0.5 mg/L, respectively. Therefore, it is of great importance for us to research on how to efficiently and economically treat Cr(VI) wastewaters.

One of the preferred methods to treat Cr(VI) in water is to convert it into less toxic Cr(III), which can be precipitated as Cr(OH)<sub>3</sub> in neutral or alkaline solutions ( $K_{sp}^{\theta}(\text{Cr(OH)}_3) = 6.3 \times 10^{-31}$ ) and removed as a solid waste [1–10]. However, the conventional

chemical reduction methods need massive use of reducing agents such as ferrous sulfate, sodium hydrogensulfite, sodium pyrosulfite, hydrazine hydrate, or sulfur dioxide, etc. which are not cost-effective. In comparison with the conventional chemical reduction methods, the semiconductor-mediated photocatalytic reduction of aqueous Cr(VI) has some obvious advantages, such as simple operation, ambient conditions, low cost, high efficiency, reusability, direct use of infinite, clean and safe natural solar energy, and no use and no release of other unwanted chemicals [1–10]. Consequently, the semiconductor-mediated photocatalytic reduction method is widely regarded as a promising way in treating aqueous Cr(VI) [1–10].

The development of high performance photocatalysts is essential for the popularization and application of photocatalysis technique in large-scale wastewater treatment. Compared with manipulating single semiconductor, the combination between two different semiconductors has proved to be successful in developing higher performance photocatalysts [11–17]. The improved photocatalytic activity of composite semiconductors is largely attributed to the enhanced separation of photoinduced electrons and holes through interfacial charge transfer [11–17]. Thus, the heterointerface between composite semiconductors which serves as the channels of interfacial charge transfer is quite important.

\* Corresponding author. Tel.: +86 0514 87962581; fax: +86 0514 87975244.  
E-mail address: [zhangyc@yzu.edu.cn](mailto:zhangyc@yzu.edu.cn) (Y.C. Zhang).

**Table 1**

The abbreviated names and properties of the as-synthesized products. Note: TBT = tetrabutyl titanate; TAA = thioacetamide; SA = surface area; DAA = dark adsorption amount for aqueous Cr (VI).

Name	SnCl <sub>4</sub> ·5H <sub>2</sub> O (mmol)	TBT (mL)	TAA (mmol)	TiO <sub>2</sub> (mass%)	BET SA (m <sup>2</sup> /g)	DAA (%)	E <sub>g</sub> (eV)	k × 10 <sup>2</sup> (min <sup>-1</sup> )
SnS <sub>2</sub>	3	0	7.5	0	22.920	3.6	2.25	0.603
SnS <sub>2</sub> /TiO <sub>2</sub> -A	3	0.5	7.5	11.2	62.291	8.6	2.31	2.459
SnS <sub>2</sub> /TiO <sub>2</sub> -B	3	1.0	7.5	31.5	67.872	13.9	2.32	4.015
SnS <sub>2</sub> /TiO <sub>2</sub> -C	3	1.5	7.5	38.2	94.399	16.5	2.32	4.106
SnS <sub>2</sub> /TiO <sub>2</sub> -D	3	2.0	7.5	44.5	97.019	19.0	2.33	4.812
SnS <sub>2</sub> /TiO <sub>2</sub> -E	3	3.0	7.5	56.3	130.697	22.4	2.34	3.686
SnS <sub>2</sub> /TiO <sub>2</sub> -F	3	4.0	7.5	60.7	135.549	26.8	2.34	3.088
TiO <sub>2</sub>	0	2	0	100	134.981	22.3	3.27	0.113

The traditional way to prepare composite photocatalysts is the simple physical mixing of two different semiconductors. However, the particles of the physically mixed two semiconductors are not tightly attached to each other and tend to separate and self-agglomerate when suspended in the solution. The heterointerface arises only when the particles of the physically mixed two semiconductors collide. As a result, the probability of interfacial charge transfer and separation in the physically mixed composite semiconductors is very low. In contrast, the in situ chemical methods are capable of preparing composite semiconductors with more uniform and thorough mixing, closer contact and even stronger interaction, which can provide tight heterointerface for charge transfer and reduce the separation and self-agglomeration of two components [11–17]. Accordingly, the composite photocatalysts synthesized via the in situ chemical methods often demonstrated superior photocatalytic performances [11–17]. Moreover, one-step synthesis outmatched two-step process in easier realization of the abovementioned advantages of the in situ chemical methods [16].

The semiconducting SnS<sub>2</sub> and TiO<sub>2</sub> with the band gaps of about 2.2 and 3.2 eV, respectively, are among the very limited options of photocatalysts suitable for practical applications, by virtue of their low cost, innocuity, high photocatalytic activity and good stability [17–19]. They have matched band potentials, that is, both the valence band and conduction band potentials of SnS<sub>2</sub> are more negative than those of TiO<sub>2</sub> [17]. This thermodynamically allows the photogenerated electron transfer from the conduction band of SnS<sub>2</sub> to the conduction band of TiO<sub>2</sub> under visible light ( $\lambda > 420$  nm) irradiation, which can enhance the separation of photogenerated electrons and holes in SnS<sub>2</sub> and bring about the sensitization of TiO<sub>2</sub>. Thus, it is feasible for SnS<sub>2</sub>/TiO<sub>2</sub> composites with appropriate compositions to possess higher visible light-driven photocatalytic activity than individual SnS<sub>2</sub> and TiO<sub>2</sub>. In addition, TiO<sub>2</sub> is cheaper than SnS<sub>2</sub>, so their combination will enable the cost reduction as compared to sole SnS<sub>2</sub> photocatalyst. However, to our knowledge, there is still no report about the use of SnS<sub>2</sub>/TiO<sub>2</sub> composite as photocatalyst in treating aqueous Cr(VI) so far.

Herein, a simple and cost-effective one-step in situ solvothermal route, which is based on the reactions of SnCl<sub>4</sub>·5H<sub>2</sub>O, thioacetamide and different amounts of tetrabutyl titanate in the mixed solvents of ethanol and acetic acid in autoclaves at 180 °C for 12 h, is proposed for the synthesis of composition-tunable SnS<sub>2</sub>/TiO<sub>2</sub> nanocomposites. The structures, compositions, BET specific surface areas and optical properties of the as-synthesized products are characterized by X-ray diffraction, energy dispersive X-ray spectroscopy, X-ray photoelectron spectroscopy, field emission scanning electron microscopy, high-resolution transmission electron microscopy, N<sub>2</sub> adsorption and UV–vis diffuse reflectance spectra, and their photocatalytic properties are tested for the reduction of aqueous Cr(VI) under visible light ( $\lambda > 420$  nm) irradiation. Furthermore, contrast photocatalytic experiments are also conducted for different doses of the as-synthesized SnS<sub>2</sub>/TiO<sub>2</sub> nanocomposite, SnS<sub>2</sub> and physical mixture of SnS<sub>2</sub> and TiO<sub>2</sub>. Meanwhile, the reasons accounting for the photocatalytic results are also discussed.

## 2. Experimental

All the reagents used were of analytical grade and purchased from Sinopharm Chemical Reagent Co., Ltd.

### 2.1. Synthesis

In synthesizing SnS<sub>2</sub>/TiO<sub>2</sub> nanocomposites, 3.0 mmol SnCl<sub>4</sub>·5H<sub>2</sub>O was weighed into 50 mL Teflon-lined stainless steel autoclaves, and subsequently the mixed solvents comprising 2.0 mL of acetic acid and a suitable amount (the total volume of ethanol and tetrabutyl titanate was 38.0 mL) of ethanol were added with stirring. After the dissolution of SnCl<sub>4</sub>·5H<sub>2</sub>O, 0.5–4.0 mL of tetrabutyl titanate and 7.5 mmol thioacetamide were added in sequence with stirring. The autoclaves were sealed and heated in an electric oven at 180 °C for 12 h, then cooled to ambient temperature naturally. The resultant precipitates were filtered, washed with deionized water, and dried in vacuum at 100 °C for 4 h.

SnS<sub>2</sub> and TiO<sub>2</sub> were synthesized respectively via the solvothermal reactions of (3.0 mmol SnCl<sub>4</sub>·5H<sub>2</sub>O + 2.0 mL acetic acid + 38.0 mL ethanol + 7.5 mmol thioacetamide) and (2.0 mL tetrabutyl titanate + 2.0 mL acetic acid + 36.0 mL ethanol) at 180 °C for 12 h.

For the convenience of description, the as-synthesized products were hereinafter called as “SnS<sub>2</sub>”, “SnS<sub>2</sub>/TiO<sub>2</sub>-A–F” and “TiO<sub>2</sub>”, as shown in Table 1.

### 2.2. Characterization

The as-synthesized products were characterized by X-ray diffraction (XRD, German Bruker AXS D8 ADVANCE X-ray diffractometer), X-ray photoelectron spectroscopy (XPS, American Thermo-VG Scientific ESCALAB 250 XPS system, Al K $\alpha$  radiation and C 1s peak (284.6 eV) reference), field emission scanning electron microscopy (FESEM) and energy dispersive X-ray spectroscopy (EDX) (Japan Hitachi S-4800 field emission scanning electron microscopy), high-resolution transmission electron microscopy (HRTEM, American FEI Tecnai G<sup>2</sup> F30 S-TWIN field-emission transmission electron microscopy), BET specific surface areas (American Micromeritics Instrument Corporation TriStar II 3020 surface area and porosity analyzer), and UV–vis diffuse reflectance spectra (American Varian Cary 5000 UV–vis–NIR spectrophotometer).

### 2.3. Photocatalytic tests

Photocatalytic properties of the as-synthesized products were tested by the reduction of aqueous Cr(VI) under visible light ( $\lambda > 420$  nm) irradiation in our homemade photochemical reactor (Electronic Supplementary materials, Fig. S1). The detailed procedure was as described in our earlier report [18]. The reduction ratio of Cr(VI) was calculated using the following expression:

$$\text{Reduction ratio of Cr(VI)} = \frac{A_0 - A_t}{A_0} \times 100\%$$

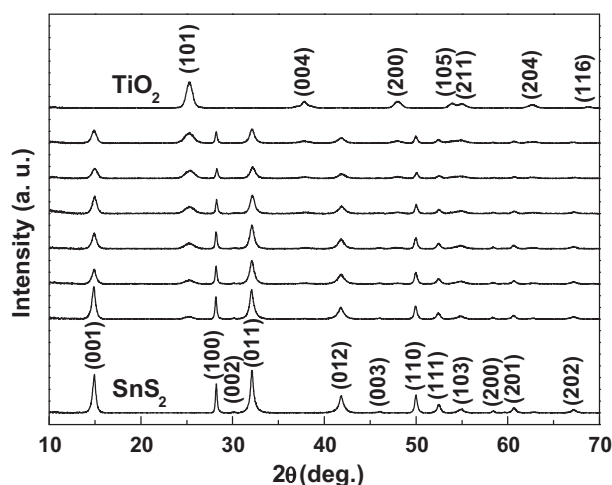


**Fig. 1.** XRD patterns of the as-synthesized products, which are in turn  $\text{SnS}_2$ ,  $\text{SnS}_2/\text{TiO}_2$ -A,  $\text{SnS}_2/\text{TiO}_2$ -B,  $\text{SnS}_2/\text{TiO}_2$ -C,  $\text{SnS}_2/\text{TiO}_2$ -D,  $\text{SnS}_2/\text{TiO}_2$ -E,  $\text{SnS}_2/\text{TiO}_2$ -F and  $\text{TiO}_2$  from the bottom up.

where  $A_0$  and  $A_t$  are the absorbance intensities when illuminated for 0 (that is, just after the dark adsorption) and  $t$  min, respectively.

### 3. Results and discussion

#### 3.1. Structural and compositional characterization

**Fig. 1** shows the XRD patterns of the as-synthesized  $\text{SnS}_2$ ,  $\text{SnS}_2/\text{TiO}_2$ -A–F and  $\text{TiO}_2$ . While the XRD peaks of  $\text{SnS}_2$  and  $\text{TiO}_2$  could be indexed to pure hexagonal phase  $\text{SnS}_2$  (berndtite-2H, JCPDS card no. 01-089-2358) and tetragonal phase  $\text{TiO}_2$  (anatase, JCPDS card no. 01-078-2486), respectively, those of  $\text{SnS}_2/\text{TiO}_2$ -A–F indicated the formation of  $\text{SnS}_2$  and  $\text{TiO}_2$  mixtures. The  $\text{TiO}_2$  contents in the as-synthesized  $\text{SnS}_2/\text{TiO}_2$  composites were determined by EDX, and the obtained results are shown in **Table 1**.

**Fig. 2** shows the XPS spectra of the as-synthesized  $\text{SnS}_2$ ,  $\text{SnS}_2/\text{TiO}_2$ -D and  $\text{TiO}_2$ . The XPS survey spectra revealed that all the samples were composed of their respective component elements. The binding energies of Sn  $3d_{5/2}$  (486.67 eV) and S  $2p_{3/2}$  (161.71 eV) of  $\text{SnS}_2$  and Ti  $2p_{3/2}$  (458.43 eV) and O 1s (529.62 eV) of  $\text{TiO}_2$  all accorded with the reference values for  $\text{SnS}_2$  and  $\text{TiO}_2$  [20–26]. Nevertheless, the binding energies of Sn  $3d_{5/2}$  (486.11 eV) and S  $2p_{3/2}$  (161.08 eV) of  $\text{SnS}_2/\text{TiO}_2$ -D showed distinct decrease as compared with those of  $\text{SnS}_2$ , while its Ti  $2p_{3/2}$  (458.60 eV) and O 1s (529.91 eV) binding energies showed slight increase as compared with those of  $\text{TiO}_2$ . This phenomenon did not happen for the  $\text{SnS}_2/\text{TiO}_2$  composite prepared by simple physical mixing of  $\text{SnS}_2$  and  $\text{TiO}_2$ , suggesting that there may exist strong interactions between the two components of  $\text{SnS}_2/\text{TiO}_2$ -D.

**Fig. 3** shows the FESEM images of the as-synthesized  $\text{SnS}_2$ ,  $\text{SnS}_2/\text{TiO}_2$ -A–F and  $\text{TiO}_2$ . As can be seen from the FESEM images of  $\text{SnS}_2$  and  $\text{TiO}_2$ ,  $\text{SnS}_2$  comprised mainly assemblies of nanoflakes (the thickness of the nanoflakes was about 21–28 nm), whereas  $\text{TiO}_2$  comprised mainly aggregates of nanoparticles (the size of the nanoparticles was estimated to be about 7–12 nm from their HRTEM image (not shown here)). As for  $\text{SnS}_2/\text{TiO}_2$ -A–F, they perhaps all comprised agglomerations of nanoflakes and nanoparticles. But from the low magnification FESEM images, the nanoflakes gradually became unobservable with the increase of  $\text{TiO}_2$  contents in these composite products. This was probably owing to the following two reasons: first, the addition of tetrabutyl titanate to the reaction solutions affected the nucleation and crystal growth processes of  $\text{SnS}_2$  under the solvothermal condition, resulting in the morphology and size change of  $\text{SnS}_2$  nanoflakes; second,  $\text{SnS}_2$

nanoflakes might be increasingly covered by the more and more amounts of  $\text{TiO}_2$  nanoparticles from  $\text{SnS}_2/\text{TiO}_2$ -A to  $\text{SnS}_2/\text{TiO}_2$ -F.

The microstructure of  $\text{SnS}_2/\text{TiO}_2$ -D was further characterized by means of TEM and HRTEM. The TEM image (**Fig. 4(a)**) disclosed that  $\text{SnS}_2/\text{TiO}_2$ -D comprised nanoflakes covered with smaller-sized nanoparticles. The HRTEM image (**Fig. 4(b)**) displayed clear lattice fringes, suggesting the crystalline nature of  $\text{SnS}_2/\text{TiO}_2$ -D. The fringe interval of 0.316 nm of the nanoflake was in accordance with the interplanar spacing of (100) crystal planes of hexagonal phase  $\text{SnS}_2$ ; whereas that of 0.352 nm of the two smaller-sized nanocrystals corresponded to the interplanar spacing of (101) crystal planes of tetragonal phase  $\text{TiO}_2$ . Thus, the TEM and HRTEM characterizations clearly demonstrated the formation of  $\text{SnS}_2/\text{TiO}_2$  heterojunction. Moreover, the heterojunction structure of  $\text{SnS}_2/\text{TiO}_2$ -D was very stable, because its TEM and HRTEM images were taken after intense ultrasonic dispersion in ethanol for 60 min. The tight heterojunction structure of  $\text{SnS}_2/\text{TiO}_2$ -D would make the interfacial electron transfer spatially available and smooth, and accordingly increase the photocatalytic activity [11–17].

#### 3.2. BET specific surface areas

The BET specific surface areas of the as-synthesized  $\text{SnS}_2$ ,  $\text{SnS}_2/\text{TiO}_2$ -A–F and  $\text{TiO}_2$  were determined by  $\text{N}_2$  adsorption, and the obtained results are presented in **Table 1**. It can be seen from **Table 1** that the values of the BET specific surface areas of the as-synthesized products followed the order of  $\text{SnS}_2/\text{TiO}_2$ -F >  $\text{TiO}_2$  >  $\text{SnS}_2/\text{TiO}_2$ -E >  $\text{SnS}_2/\text{TiO}_2$ -D >  $\text{SnS}_2/\text{TiO}_2$ -C >  $\text{SnS}_2/\text{TiO}_2$ -B >  $\text{SnS}_2/\text{TiO}_2$ -A >  $\text{SnS}_2$ .

#### 3.3. Optical properties

The UV–vis diffuse reflectance spectra of the as-synthesized  $\text{SnS}_2$ ,  $\text{SnS}_2/\text{TiO}_2$ -A–F and  $\text{TiO}_2$  were measured and converted into the absorption mode (**Fig. 5**) using the Kubelka–Munk function [26–29]:

$$F(R_\infty) = \frac{(1 - R_\infty)^2}{2R_\infty} = \frac{\alpha}{S}$$

$$R_\infty = \frac{R_{\text{sample}}}{R_{\text{BaSO}_4}}$$

where  $F(R_\infty)$ ,  $R$ ,  $\alpha$  and  $S$  are the Kubelka–Munk function, reflectance, absorption coefficient and scattering coefficient, respectively. As can be seen from **Fig. 5**,  $\text{SnS}_2/\text{TiO}_2$ -A–F, like  $\text{SnS}_2$ , displayed light-absorbing abilities nearly in the entire visible light region, implying that they have the potential to be efficient visible light-driven photocatalysts. But in the UV region where the photoabsorption by  $\text{TiO}_2$  occurred, the photoabsorption profiles of  $\text{SnS}_2/\text{TiO}_2$ -A–F are somewhat different from that of  $\text{SnS}_2$ , owing to the overlap of the photoabsorption by  $\text{SnS}_2$  and  $\text{TiO}_2$ . The band gaps ( $E_g$ ) of the as-synthesized products were estimated from their optical absorption edges using the following equation:

$$\alpha h\nu = B(h\nu - E_g)^{1/2}$$

where  $h\nu$  and  $B$  are discrete photon energy and a constant relative to the material, respectively. For the diffused reflectance spectra,  $F(R_\infty)$  can be used instead of  $\alpha$  [26–29]. So, the curves of  $(F(R_\infty)h\nu)^2$  vs  $(h\nu)$  for the as-synthesized products are plotted in **Fig. S2**. By extrapolating the linear portion of the  $(F(R_\infty)h\nu)^2$  vs  $(h\nu)$  curves to  $(F(R_\infty)h\nu)^2 = 0$ , the  $E_g$  values of  $\text{SnS}_2$ ,  $\text{SnS}_2/\text{TiO}_2$ -A–F and  $\text{TiO}_2$  are obtained and shown in **Table 1**.

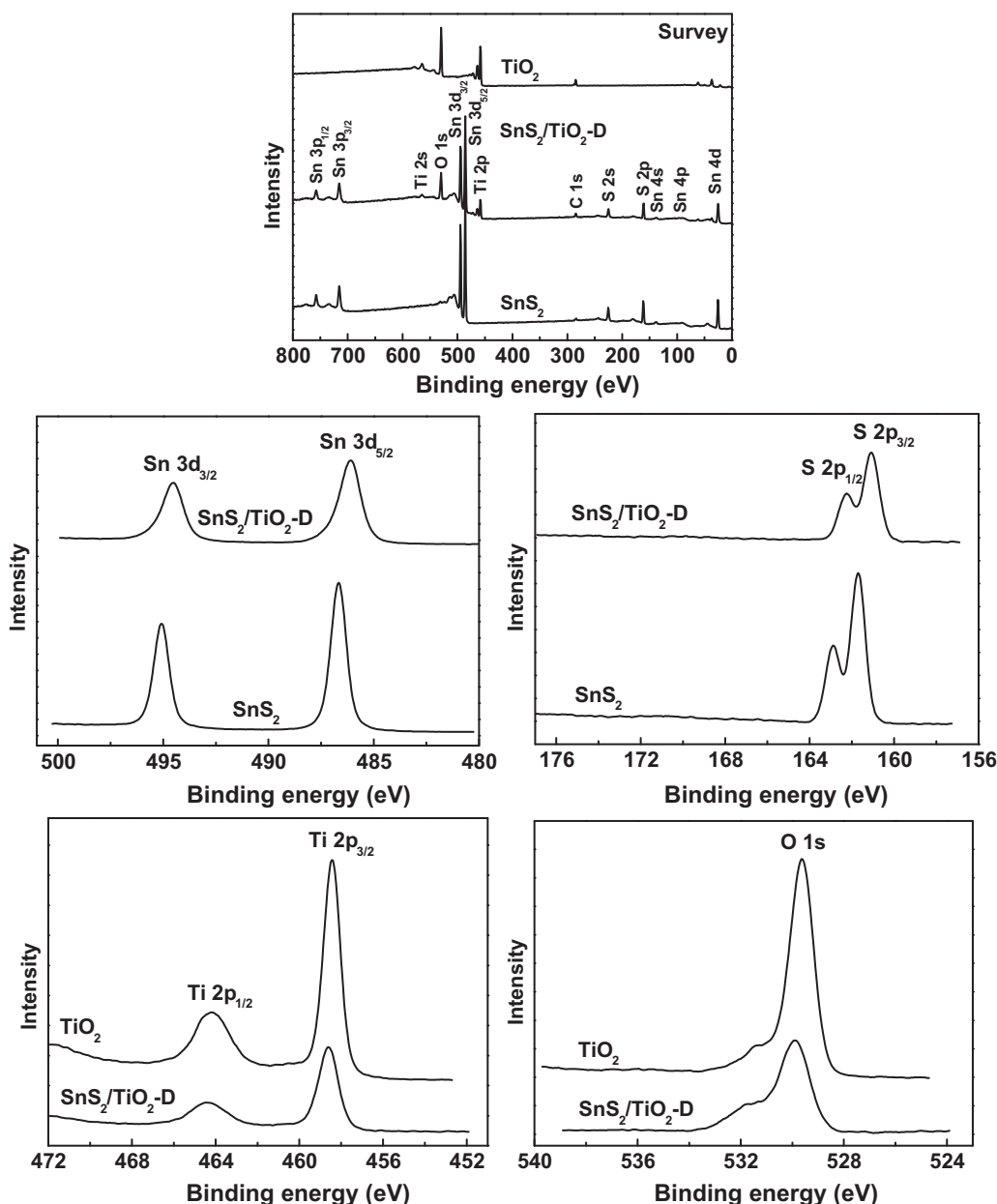


Fig. 2. XPS spectra of  $\text{SnS}_2$ ,  $\text{SnS}_2/\text{TiO}_2\text{-D}$  and  $\text{TiO}_2$ .

### 3.4. Photocatalytic tests

#### 3.4.1. Photocatalytic activities

Fig. 6 shows the photocatalytic activities of the as-synthesized  $\text{SnS}_2$ ,  $\text{SnS}_2/\text{TiO}_2\text{-A-F}$  and  $\text{TiO}_2$  as well as the commercial P25  $\text{TiO}_2$  in the reduction of aqueous  $\text{Cr(VI)}$  under visible light ( $\lambda > 420 \text{ nm}$ ) irradiation. As can be seen from Fig. 6, in the presence of P25  $\text{TiO}_2$  or in the absence of any photocatalyst, the reduction of  $\text{Cr(VI)}$  hardly occurred when subjected to visible light ( $\lambda > 420 \text{ nm}$ ) irradiation for 120 min. In contrast, the reduction ratios of  $\text{Cr(VI)}$  increased with the increase of irradiation time in the presence of  $\text{SnS}_2/\text{TiO}_2\text{-A-F}$ ,  $\text{SnS}_2$  and  $\text{TiO}_2$ , indicating that all our products possessed photocatalytic activities in the reduction of aqueous  $\text{Cr(VI)}$  under visible light ( $\lambda > 420 \text{ nm}$ ) irradiation. Nevertheless, the photocatalytic activities of  $\text{SnS}_2/\text{TiO}_2\text{-A-F}$  were obviously much higher than those of  $\text{SnS}_2$  and  $\text{TiO}_2$ . To quantitatively compare their photocatalytic activities, the reaction rate constants ( $k$ ) for the photocatalytic reduction reactions over different samples

were calculated by adopting the pseudo-first-order model [30–34]:

$$\ln \left( \frac{C_0}{C} \right) = kt$$

where  $C_0$  and  $C$  are the concentrations of aqueous  $\text{Cr(VI)}$  when illuminated for 0 and  $t$  min, respectively. The plots of  $\ln(C_0/C)$  versus irradiation time ( $t$ ) and the corresponding values of  $k$  and correlation coefficient ( $R^2$ ) for all sets of the photocatalytic reduction reactions are provided in Fig. S3. It was observed that the photocatalytic activities of the as-synthesized products followed the order of  $\text{SnS}_2/\text{TiO}_2\text{-D} > \text{SnS}_2/\text{TiO}_2\text{-C} > \text{SnS}_2/\text{TiO}_2\text{-B} > \text{SnS}_2/\text{TiO}_2\text{-E} > \text{SnS}_2/\text{TiO}_2\text{-F} > \text{SnS}_2/\text{TiO}_2\text{-A} > \text{SnS}_2 > \text{TiO}_2$ . These photocatalytic results can be rationally explained as follows.

#### 3.4.2. Photocatalytic mechanism

In principle, when semiconductor photocatalysts are irradiated by the light with photon energies greater than or equal to their

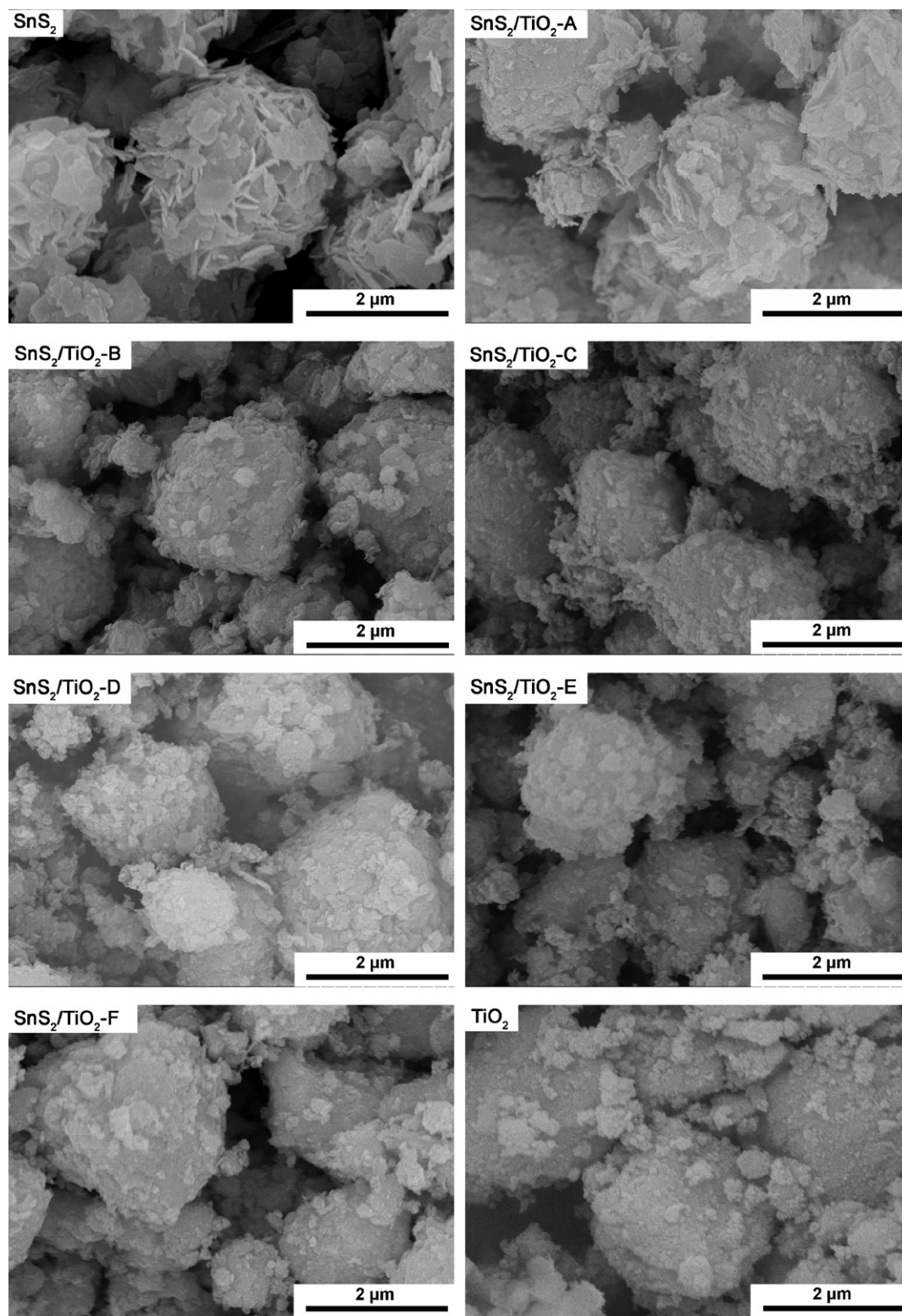
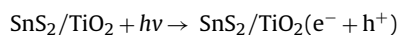
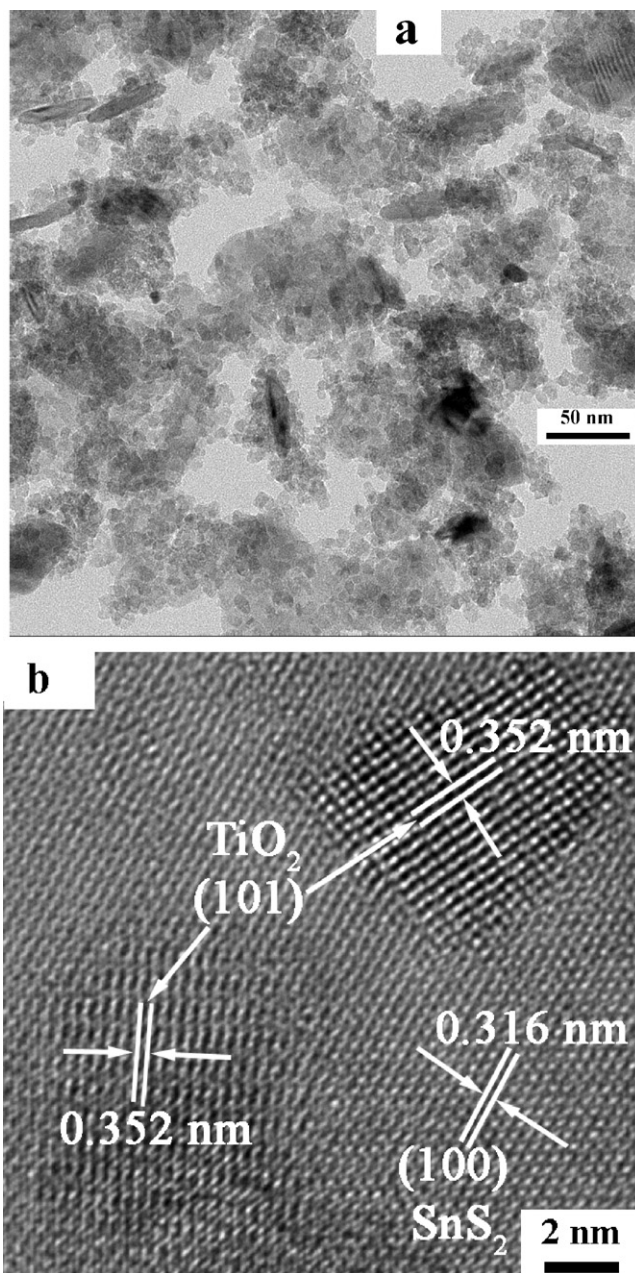


Fig. 3. FESEM images of  $\text{SnS}_2$ ,  $\text{SnS}_2/\text{TiO}_2$ -A–F and  $\text{TiO}_2$ .

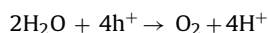
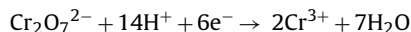
band gaps, the electrons in their valence bands can be excited to their conduction bands, simultaneously leaving behind an equal amount of electron vacancies or “holes” in their valence bands. A portion of the photogenerated electrons ( $e^-$ ) and holes ( $h^+$ ) may migrate to the catalyst surface and participate in the reduction and oxidation reactions with adsorbed species, respectively. In our case of  $\text{SnS}_2/\text{TiO}_2$ -mediated photocatalytic reduction of aqueous

$\text{Cr(VI)}$ , no extra reducing agents or hole scavengers were added. Presumably, the photogenerated electrons reduced  $\text{Cr}_2\text{O}_7^{2-}$  to  $\text{Cr(III)}$ , meanwhile the holes oxidized water to  $\text{O}_2$  [34–41]. The possible reactions involved might be described as follows:





**Fig. 4.** (a) TEM and (b) HRTEM images of  $\text{SnS}_2/\text{TiO}_2\text{-D}$  taken after intense ultrasonic dispersion in ethanol for 60 min.



For  $\text{SnS}_2/\text{TiO}_2$  nanocomposites upon visible light ( $\lambda > 420 \text{ nm}$ ) irradiation, the electrons in the valence band of  $\text{SnS}_2$  can be excited to its conduction band with simultaneous generation of an equal amount of holes in its valence band, while  $\text{TiO}_2$  has little response ability due to its wide band gap ( $E_g = 3.27 \text{ eV}$ ). Because the valence band and conduction band potentials of  $\text{SnS}_2$  are more negative than those of  $\text{TiO}_2$  [17], the photogenerated electrons can migrate from the conduction band of  $\text{SnS}_2$  to the conduction band of  $\text{TiO}_2$ , whereas the photogenerated holes still remain on the valence band of  $\text{SnS}_2$  (Fig. S4). Thus, the photogenerated electrons and holes in  $\text{SnS}_2$  can be effectively separated, and accordingly their recombination is slowed down. The efficient charge separation

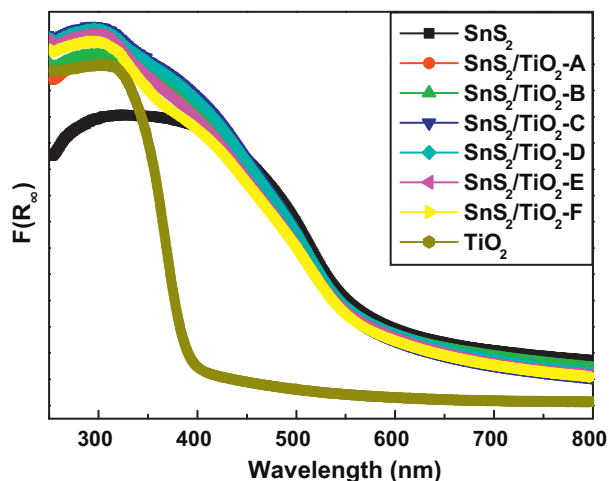


**Fig. 5.** UV-vis diffuse reflectance spectra of  $\text{SnS}_2$ ,  $\text{SnS}_2/\text{TiO}_2\text{-A-F}$  and  $\text{TiO}_2$ .

can increase the lifetime of the charge carriers and enhance the efficiency of the interfacial charge transfer to adsorbed substrates [42–49]. Moreover,  $\text{TiO}_2$  can be sensitized via the aforementioned electron transfer process. Hence, it is reasonable that  $\text{SnS}_2/\text{TiO}_2\text{-A-F}$  can exhibit higher photocatalytic efficiencies than sole  $\text{SnS}_2$  and  $\text{TiO}_2$ .

As for the difference in the photocatalytic activities of  $\text{SnS}_2/\text{TiO}_2\text{-A-F}$ , it was most likely a result of the combined action of many factors, such as composition, specific surface area, adsorption capacity for  $\text{Cr(VI)}$ , morphology, size, crystallinity, crystal defects, band gap, dispersibility and suspensibility, etc. However, because there was no direct proportion between the data of the above-mentioned influencing factors and the photocatalytic activities of  $\text{SnS}_2/\text{TiO}_2\text{-A-F}$  (Table 1), and almost all the other factors are actually bound up with the composition of  $\text{SnS}_2/\text{TiO}_2$  nanocomposites, we believed that the composition of  $\text{SnS}_2/\text{TiO}_2$  nanocomposites should play a predominant role in their photocatalytic activities. On one hand, when the contents of  $\text{TiO}_2$  in the  $\text{SnS}_2/\text{TiO}_2$  nanocomposites were too low (e.g.,  $\text{SnS}_2/\text{TiO}_2\text{-A-C}$ ), a portion of  $\text{SnS}_2$  would have no chance of contacting  $\text{TiO}_2$  (or in other words, the surfaces of a portion of  $\text{SnS}_2$  nanoflakes are either “bare” or “insufficiently covered” with  $\text{TiO}_2$  nanoparticles), which restricted the efficient interfacial electron transfer from  $\text{SnS}_2$  to  $\text{TiO}_2$ . As a result, their photocatalytic activities cannot be enhanced to the greatest extent. On

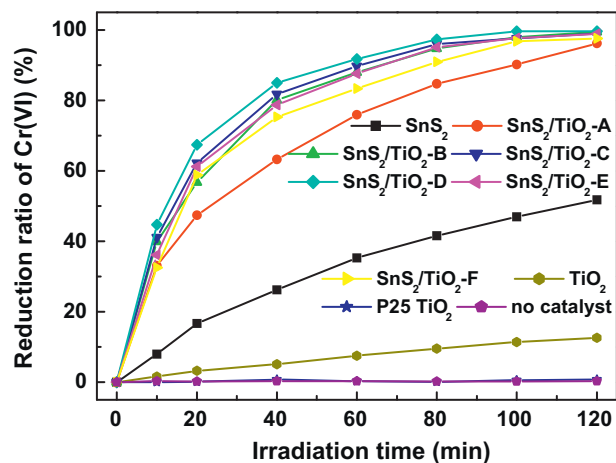


**Fig. 6.** Photocatalytic activities of the as-synthesized  $\text{SnS}_2$ ,  $\text{SnS}_2/\text{TiO}_2\text{-A-F}$  and  $\text{TiO}_2$  as well as the commercial P25  $\text{TiO}_2$  in the reduction of aqueous  $\text{Cr(VI)}$  under visible light ( $\lambda > 420 \text{ nm}$ ) irradiation.

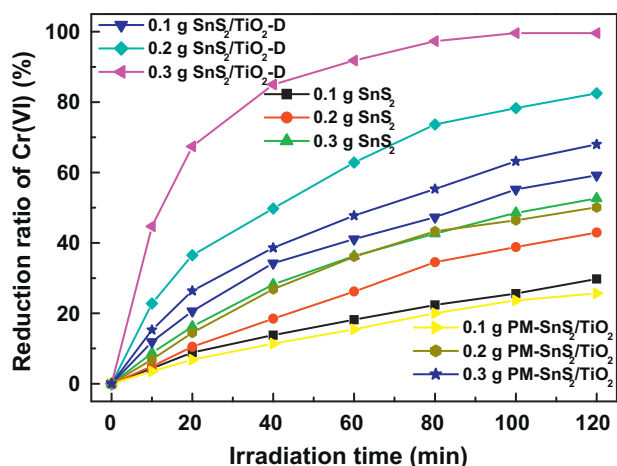


**Fig. 7.** Comparison of the photocatalytic efficiencies of 0.1–0.3 g of  $\text{SnS}_2$ ,  $\text{SnS}_2/\text{TiO}_2$ -D and PM- $\text{SnS}_2/\text{TiO}_2$  (PM- $\text{SnS}_2/\text{TiO}_2$  is the abbreviation for the  $\text{SnS}_2/\text{TiO}_2$  composite prepared by the physical mixing method: suitable amounts (55.5 mass%  $\text{SnS}_2$  and 44.5 mass%  $\text{TiO}_2$ , the same composition as  $\text{SnS}_2/\text{TiO}_2$ -D) of the as-synthesized  $\text{SnS}_2$  and  $\text{TiO}_2$  were mixed by manual grinding for 15 min in an agate mortar).

the other hand, too high  $\text{TiO}_2$  contents in the  $\text{SnS}_2/\text{TiO}_2$  nanocomposites (e.g.,  $\text{SnS}_2/\text{TiO}_2$ -E and  $\text{SnS}_2/\text{TiO}_2$ -F) were also detrimental to maximize their photocatalytic activities. This was mainly because that  $\text{SnS}_2$  possessed a much higher photocatalytic activity than  $\text{TiO}_2$  under visible light ( $\lambda > 420 \text{ nm}$ ) irradiation. The more content of  $\text{TiO}_2$  meant the less content of  $\text{SnS}_2$  in the  $\text{SnS}_2/\text{TiO}_2$  nanocomposites, whose dose for each photocatalytic experiment was fixed at 0.3 g. The lower amount of more active  $\text{SnS}_2$  involved in the photocatalytic processes would bring about lower photocatalytic efficiencies, because the photocatalytic efficiencies of both  $\text{SnS}_2$  and  $\text{SnS}_2/\text{TiO}_2$  nanocomposites were directly proportional to their doses as shown later in Fig. 7. Moreover, a portion of  $\text{TiO}_2$  nanoparticles can no more be attached to the surfaces of limited  $\text{SnS}_2$  nanoflakes, as the  $\text{TiO}_2$  content in  $\text{SnS}_2/\text{TiO}_2$  nanocomposites was too high. Besides, too much  $\text{TiO}_2$  on  $\text{SnS}_2$  surface possibly blocked the light irradiation on  $\text{SnS}_2$  and hindered the contact of  $\text{SnS}_2$  with aqueous  $\text{Cr(VI)}$ . Therefore, there must exist an optimum composition for  $\text{SnS}_2/\text{TiO}_2$  nanocomposite to achieve the highest photocatalytic activity. For the reasons discussed above,  $\text{SnS}_2/\text{TiO}_2$ -D with a suitable content (44.5 mass%) of  $\text{TiO}_2$  possessed the highest photocatalytic activity among  $\text{SnS}_2/\text{TiO}_2$ -A–F.

### 3.4.3. Influence of interface

In order to illustrate the influence and significance of the interface between the two components of  $\text{SnS}_2/\text{TiO}_2$  nanocomposites, the photocatalytic efficiencies of 0.1–0.3 g of  $\text{SnS}_2$ ,  $\text{SnS}_2/\text{TiO}_2$ -D and PM- $\text{SnS}_2/\text{TiO}_2$  were further compared. As can be seen from Fig. 7 and Fig. S3, 0.1–0.3 g of  $\text{SnS}_2/\text{TiO}_2$ -D always exhibited much higher photocatalytic efficiencies than the same doses of  $\text{SnS}_2$  and PM- $\text{SnS}_2/\text{TiO}_2$ . Nevertheless, the comparison between  $\text{SnS}_2$  and PM- $\text{SnS}_2/\text{TiO}_2$  gave a dose-dependent result: while 0.2–0.3 g of PM- $\text{SnS}_2/\text{TiO}_2$  exhibited higher photocatalytic efficiencies than the same doses of  $\text{SnS}_2$ , an opposite conclusion was drawn when their dose was decreased to 0.1 g. The foregoing results definitely manifest that the interface between the two components of  $\text{SnS}_2/\text{TiO}_2$  nanocomposites played an important role in their photocatalytic activity. When larger concentrations (e.g., 0.2–0.3 g) of PM- $\text{SnS}_2/\text{TiO}_2$  were suspended in the  $\text{Cr(VI)}$  aqueous solution with continuous magnetic stirring, there was still great chance for the isolated  $\text{SnS}_2$  and  $\text{TiO}_2$  particles to collide with each other to induce the instantaneous interface. Accordingly, the probability of photogenerated electron transfer and charge separation was also relatively high, rendering PM- $\text{SnS}_2/\text{TiO}_2$  possess superior

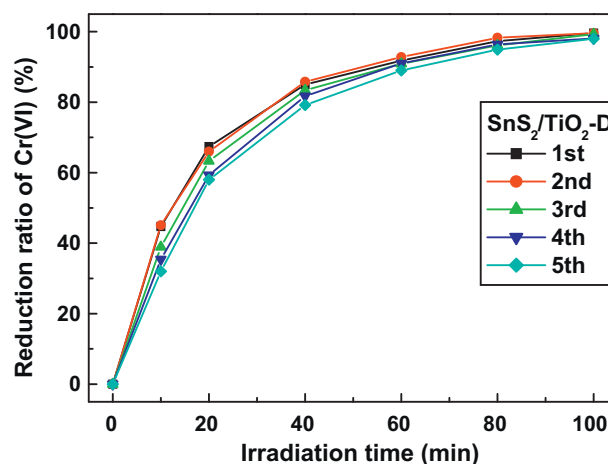


**Fig. 8.** Photocatalytic performances of  $\text{SnS}_2/\text{TiO}_2$ -D in the first five reuse cycles.

photocatalytic activity to  $\text{SnS}_2$  in the cases of larger doses. Otherwise, when the concentration of PM- $\text{SnS}_2/\text{TiO}_2$  was too small, the chance of mutual collision between isolated  $\text{SnS}_2$  and  $\text{TiO}_2$  particles and subsequent interfacial electron transfer became much less, causing 0.1 g of PM- $\text{SnS}_2/\text{TiO}_2$  to have lower photocatalytic efficiency than the same dose of  $\text{SnS}_2$ . Compared with the instantaneous interface provided by the random collision between separated  $\text{SnS}_2$  and  $\text{TiO}_2$  particles of PM- $\text{SnS}_2/\text{TiO}_2$ , the tight heterojunction structure of  $\text{SnS}_2/\text{TiO}_2$ -D can facilitate interfacial electron transfer and reduce the separation and self-agglomeration of two components. Consequently,  $\text{SnS}_2/\text{TiO}_2$ -D performed the best under the aforementioned conditions of different doses of photocatalysts.

In addition, Fig. 7 also illustrated that the dose of  $\text{SnS}_2/\text{TiO}_2$ -D exerted a tremendous influence on its photocatalytic efficiency. With an increase in the dose of  $\text{SnS}_2/\text{TiO}_2$ -D, the reduction rate of  $\text{Cr(VI)}$  was also enhanced. The enhancement in the reduction rate of  $\text{Cr(VI)}$  with increased concentration of photocatalyst is a characteristic of heterogeneous catalysis, and can be rationalized in terms of the available active sites on the catalyst surface and the effective light penetration into the suspension [50–52].

### 3.4.4. Photocatalytic stability of $\text{SnS}_2/\text{TiO}_2$ -D

Since the stability of sulfide-based photocatalysts has always been a concern, it is important to investigate the stability and reusability of  $\text{SnS}_2/\text{TiO}_2$  nanocomposite in photocatalytic reduction of aqueous  $\text{Cr(VI)}$ . So, in the current work,  $\text{SnS}_2/\text{TiO}_2$ -D was recycled for five times in the same photocatalytic reactions. After each reuse cycle which lasted 100 min, the photocatalyst was separated from the aqueous suspension by filtration, washed with 1 mol/L  $\text{HNO}_3$  aqueous solution (to reduce the amount of  $\text{Cr(OH)}_3$  deposited on the surface of  $\text{SnS}_2/\text{TiO}_2$ -D) and deionized water, dried in vacuum at  $100^\circ\text{C}$  for 4 h, and weighed for the next reuse cycle. Taking into account the mass loss of photocatalyst during each reuse cycle, the former reuse cycle must be conducted twice in order to accumulate enough samples for the latter reuse cycle. Fig. 8 shows the photocatalytic performance of  $\text{SnS}_2/\text{TiO}_2$ -D in the first five reuse cycles. Apparently,  $\text{SnS}_2/\text{TiO}_2$ -D exhibited little loss of photocatalytic activity in the first five reuse cycles. For example, even in the fifth reuse cycle of  $\text{SnS}_2/\text{TiO}_2$ -D, the reduction ratio of  $\text{Cr(VI)}$  can still reach 98% upon visible light irradiation within 100 min.

The product collected after the fifth reuse cycle of  $\text{SnS}_2/\text{TiO}_2$ -D in photocatalysis ( $\text{SnS}_2/\text{TiO}_2$ -AP) was further characterized by means of XPS. The XPS survey spectrum of  $\text{SnS}_2/\text{TiO}_2$ -AP (Fig. 9) disclosed the presence of Sn, S, Ti and O components, as well as Cr and C (C is from adsorbed gaseous molecules and usually unavoidable

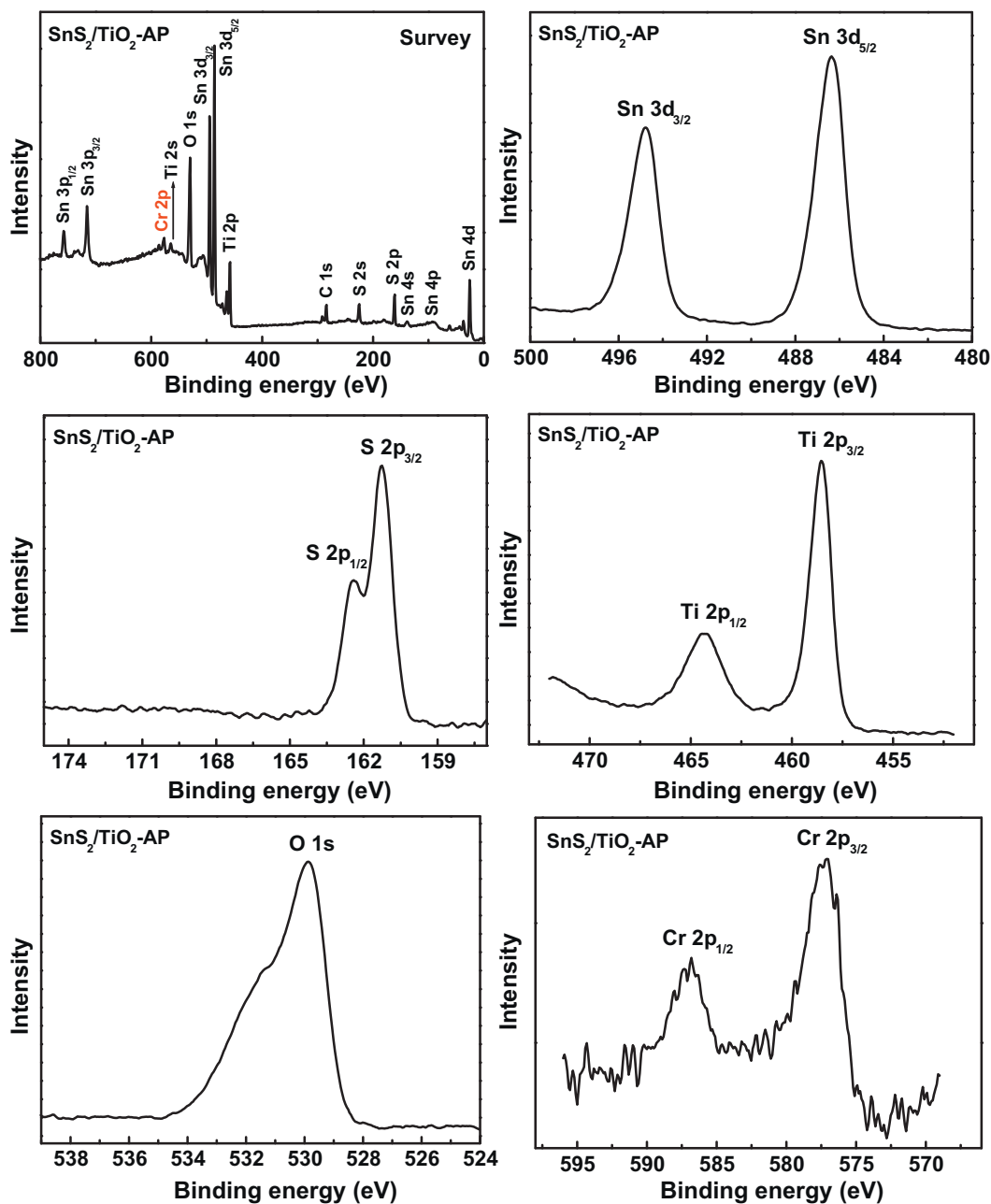


Fig. 9. XPS spectra of  $\text{SnS}_2/\text{TiO}_2\text{-AP}$ .

in XPS measurements) contaminants. The binding energies of Sn  $3d_{5/2}$ , S  $2p_{3/2}$ , Ti  $2p_{3/2}$  and O  $1s$  of  $\text{SnS}_2/\text{TiO}_2\text{-AP}$  were in turn 486.37, 161.27, 458.54 and 530.02 eV (Fig. 9), which were consistent with those of  $\text{SnS}_2/\text{TiO}_2\text{-D}$  (Fig. 2). Besides, the binding energy of Cr  $2p_{3/2}$  of  $\text{SnS}_2/\text{TiO}_2\text{-AP}$  was observed at 577.24 eV (Fig. 9), which corresponded to Cr(III) in  $\text{Cr}(\text{OH})_3$  [18,53,54]. The formation of  $\text{Cr}(\text{OH})_3$  on the surface of  $\text{SnS}_2/\text{TiO}_2\text{-AP}$  can be due to the hydrolysis-precipitation of Cr(III) cations, which were generated from the photocatalytic reduction of adsorbed Cr(VI).

#### 4. Conclusions

Composition-tunable synthesis of  $\text{SnS}_2/\text{TiO}_2$  nanocomposites was achieved via a one-step in situ solvothermal method at 180 °C, using the common and inexpensive  $\text{SnCl}_4 \cdot 5\text{H}_2\text{O}$ , thioacetamide and

tetrabutyl titanate as the reactants and ethanol–acetic acid mixture as the solvent. This method is simple, cost-effective and capable of synthesizing  $\text{SnS}_2/\text{TiO}_2$  nanocomposite with a tight heterojunction structure.

Through the photocatalytic experiments using aqueous Cr(VI) as a target contaminant under visible light ( $\lambda > 420 \text{ nm}$ ) irradiation, the following results were obtained: (1) the photocatalytic activities of  $\text{SnS}_2/\text{TiO}_2$  nanocomposites depended on their compositions, and  $\text{SnS}_2/\text{TiO}_2\text{-D}$  with a suitable content (44.5 mass%) of  $\text{TiO}_2$  possessed the highest photocatalytic activity among  $\text{SnS}_2/\text{TiO}_2\text{-A-F}$ ; (2) 0.1–0.3 g of  $\text{SnS}_2/\text{TiO}_2\text{-D}$  invariably exhibited much higher photocatalytic efficiencies than the same doses of  $\text{SnS}_2$  and PM- $\text{SnS}_2/\text{TiO}_2$ ; (3)  $\text{SnS}_2/\text{TiO}_2\text{-D}$  had good photocatalytic stability; and (4) Cr(VI) can be reduced to Cr(III) by  $\text{SnS}_2/\text{TiO}_2$ -mediated photocatalysis. Meanwhile, the reasons responsible for the photocatalytic results were also discussed. The high visible light-driven

photocatalytic activity and good stability of  $\text{SnS}_2/\text{TiO}_2$ -D render it a promising photocatalyst in efficient utilization of solar energy for the treatment of Cr(VI) wastewater.

## Acknowledgments

A Project Funded by the Priority Academic Program Development of Jiangsu Higher Education Institutions, and the Science & Technology Innovation Fund of Yangzhou University (2011CXJ012).

## Appendix A. Supplementary data

Supplementary data associated with this article can be found, in the online version, at <http://dx.doi.org/10.1016/j.apcatb.2012.04.018>.

## References

- [1] N. Wang, L. Zhu, K. Deng, Y. She, Y. Yu, H. Tang, *Applied Catalysis B* 95 (2010) 400–407.
- [2] R. Gherbi, N. Nasrallah, A. Amrane, R. Maachi, M. Trari, *Journal of Hazardous Materials* 186 (2011) 1124–1130.
- [3] G. Cappelletti, C.L. Bianchi, S. Ardizzzone, *Applied Catalysis B* 78 (2008) 193–201.
- [4] A. Kleiman, A. Márquez, M.L. Vera, J.M. Meichtry, M.I. Litter, *Applied Catalysis B* 101 (2011) 676–681.
- [5] B. Sun, E.P. Reddy, P.G. Smirniotis, *Environmental Science and Technology* 39 (2005) 6251–6259.
- [6] S. Luo, Y. Xiao, L. Yang, C. Liu, F. Su, *Separation and Purification Technology* 79 (2011) 85–91.
- [7] L. Yang, Y. Xiao, S. Liu, Y. Li, Q. Cai, S. Luo, *Applied Catalysis B* 94 (2010) 142–149.
- [8] X. Liu, L. Pan, Q. Zhao, T. Lv, G. Zhu, T. Chen, T. Lu, Z. Sun, C. Sun, *Chemical Engineering Journal* 183 (2012) 238–243.
- [9] H.T. Hsu, S.S. Chen, Y.S. Chen, *Separation and Purification Technology* 80 (2011) 663–669.
- [10] G. Kim, W. Choi, *Applied Catalysis B* 100 (2010) 77–83.
- [11] X. Lin, F. Huang, J. Xing, W. Wang, F. Xu, *Acta Materialia* 56 (2008) 2699–2705.
- [12] Y.C. Zhang, Z.N. Du, M. Zhang, *Materials Letters* 65 (2011) 2891–2894.
- [13] Y.C. Zhang, Z.N. Du, K.W. Li, M. Zhang, D.D. Dionysiou, *ACS Applied Materials & Interfaces* 3 (2011) 1528–1537.
- [14] S. Chu, X. Zheng, F. Kong, G. Wu, L. Luo, *Materials Chemistry and Physics* 129 (2011) 1184–1188.
- [15] H. Huang, D. Li, Q. Lin, W. Zhang, Y. Shao, Y. Chen, M. Sun, X. Fu, *Environmental Science and Technology* 43 (2009) 4164–4168.
- [16] S. Ding, X. Yin, X. Lü, Y. Wang, F. Huang, D. Wan, *ACS Applied Materials & Interfaces* 4 (2012) 306–311.
- [17] C. Yang, W. Wang, Z. Shan, F. Huang, *Journal of Solid State Chemistry* 182 (2009) 807–812.
- [18] Y.C. Zhang, J. Li, M. Zhang, D.D. Dionysiou, *Environmental Science and Technology* 45 (2011) 9324–9331.
- [19] R. Lucena, F. Fresno, F.C. Conesa, *Applied Catalysis A* 415–416 (2012) 111–117.
- [20] Q. Yang, K. Tang, C. Wang, D. Zhang, Y. Qian, *Journal of Solid State Chemistry* 164 (2002) 106–109.
- [21] J. Ng, X. Wang, D.D. Sun, *Applied Catalysis B* 110 (2011) 260–272.
- [22] C. Zhai, N. Du, H. Zhang, J. Yu, D. Yang, *ACS Applied Materials & Interfaces* 3 (2011) 4067–4074.
- [23] J. Liu, Y. Zhao, L. Shi, S. Yuan, J. Fang, Z. Wang, M. Zhang, *ACS Applied Materials & Interfaces* 3 (2011) 1261–1268.
- [24] Y. Ku, C.N. Lin, W.M. Hou, *Journal of Molecular Catalysis A* 349 (2011) 20–27.
- [25] J. Mu, B. Chen, M. Zhang, Z. Guo, P. Zhang, Z. Zhang, Y. Sun, C. Shao, Y. Liu, *ACS Applied Materials & Interfaces* 4 (2012) 424–430.
- [26] Y.C. Zhang, Z.N. Du, K.W. Li, M. Zhang, *Separation and Purification Technology* 81 (2011) 101–107.
- [27] D. Wodka, E. Bielańska, R.P. Socha, M.E. Wodka, J. Gurgul, P. Nowak, *ACS Applied Materials & Interfaces* 2 (2010) 1945–1953.
- [28] F. Spadavecchia, G. Cappelletti, S. Ardizzzone, C.L. Bianchi, S. Cappelli, C. Oliva, *Applied Catalysis B* 96 (2010) 314–322.
- [29] Y. Liao, W. Que, P. Zhong, J. Zhang, Y. He, *ACS Applied Materials & Interfaces* 3 (2011) 2800–2804.
- [30] F. Jiang, Z. Zheng, Z. Xu, S. Zheng, *Journal of Hazardous Materials* 134 (2006) 94–103.
- [31] N. Nasrallah, M. Kebir, Z. Koudri, M. Trari, *Journal of Hazardous Materials* 185 (2011) 1398–1404.
- [32] S.C. Xu, Y.X. Zhang, S.S. Pan, H.L. Ding, G.H. Li, *Journal of Hazardous Materials* 196 (2011) 29–35.
- [33] L. Wang, N. Wang, L. Zhu, H. Yu, H. Tang, *Journal of Hazardous Materials* 152 (2008) 93–99.
- [34] R. Mu, Z. Xu, L. Li, Y. Shao, H. Wan, S. Zheng, *Journal of Hazardous Materials* 176 (2010) 495–502.
- [35] A. Idris, N. Hassan, N.S.M. Ismail, E. Misran, N.M. Yusof, A.F. Ngomsik, A. Bee, *Water Research* 44 (2010) 1683–1688.
- [36] D.P. Das, K. Parida, B.R. De, *Journal of Molecular Catalysis A* 245 (2006) 217–224.
- [37] S. Tuprakay, W. Liengcharernsit, *Journal of Hazardous Materials* 124 (2005) 53–58.
- [38] Q.L. Yang, S.Z. Kang, H. Chen, W. Bu, J. Mu, *Desalination* 266 (2011) 149–153.
- [39] T. Aarthi, G. Madras, *Catalysis Communications* 9 (2008) 630–634.
- [40] S. Rengaraj, S. Venkataraj, J.W. Yeon, Y. Kim, X.Z. Li, G.K.H. Pang, *Applied Catalysis B* 77 (2007) 157–165.
- [41] T. Papadam, N.P. Xekoukoulotakis, I. Poullos, D. Mantzavinos, *Journal of Photochemistry and Photobiology A* 186 (2007) 308–315.
- [42] Z. Zhang, C. Shao, X. Li, C. Wang, M. Zhang, Y. Liu, *ACS Applied Materials & Interfaces* 2 (2010) 2915–2923.
- [43] L.S. Yang, S.L. Luo, Y. Li, Y. Xiao, Q. Kang, Q.Y. Cai, *Environmental Science and Technology* 44 (2010) 7641–7646.
- [44] J. Mu, C. Shao, Z. Guo, Z. Zhang, M. Zhang, P. Zhang, B. Chen, Y. Liu, *ACS Applied Materials & Interfaces* 3 (2011) 590–596.
- [45] C. Wang, L. Yin, L. Zhang, N. Liu, N. Lun, Y. Qi, *ACS Applied Materials & Interfaces* 2 (2010) 3373–3377.
- [46] W. Zhou, H. Liu, J. Wang, D. Liu, G. Du, J. Cui, *ACS Applied Materials & Interfaces* 2 (2010) 2385–2392.
- [47] V.M. Daskalaki, M. Antoniadou, G.L. Puma, D.I. Kondarides, P. Lianos, *Environmental Science and Technology* 44 (2010) 7200–7205.
- [48] Q. Li, J.K. Shang, *Environmental Science and Technology* 44 (2010) 3493–3499.
- [49] B. Liu, A. Khare, E.S. Aydil, *ACS Applied Materials & Interfaces* 3 (2011) 4444–4450.
- [50] A. Idris, N. Hassan, R. Rashid, A.-F. Ngomsik, *Journal of Hazardous Materials* 186 (2011) 629–635.
- [51] Y.C. Zhang, Z.N. Du, S.Y. Li, M. Zhang, *Applied Catalysis B* 95 (2010) 153–159.
- [52] M. Qamar, M.A. Gondal, Z.H. Yamani, *Journal of Hazardous Materials* 187 (2011) 258–263.
- [53] N. Wang, Y. Xu, L. Zhu, X. Shen, H. Tang, *Journal of Photochemistry and Photobiology A* 201 (2009) 121–127.
- [54] N. Wu, H. Wei, L. Zhang, *Environmental Science & Technology* 46 (2012) 419–425.